

## Chapter 4

### DC CHARACTERISTICS OF QWITT DEVICES

In this chapter the dc characteristics of different QWITT diodes and resonant tunneling diodes will be examined. We will discuss the use of the dc terminal characteristics as a deterministic tool to predict rf performance. This will lead to a better understanding of the relationship between measured dc characteristics and rf oscillator performance for a particular device structure.

#### 4.1 Devices with Uniformly Doped Depletion Regions

The heterolayers were grown in a Varian GEN II MBE system on n<sup>+</sup>, (100) GaAs substrates, silicon doped to  $3\text{-}5 \times 10^{18} \text{ cm}^{-3}$ . Details of the MBE growth conditions were described in the previous chapter. A schematic diagram of the device structures used in this study is shown in Fig. 4.1. Three QWITT device structures, A, B, and C, consisting of identical quantum well regions but with three different  $5 \times 10^{16} \text{ cm}^{-3}$ , n-GaAs, drift region lengths of 500Å, 1000Å, and 2000Å respectively, were examined [71]. A maximum depletion region length of 2000Å was chosen, since that corresponds to the optimum length of the drift region for 10 GHz operation based on the small signal model for the QWITT diode [64]. The quantum well regions consisted of a 50Å GaAs layer sandwiched between two AlAs layers 17Å thick. The AlAs barrier layers were kept thin to increase the current

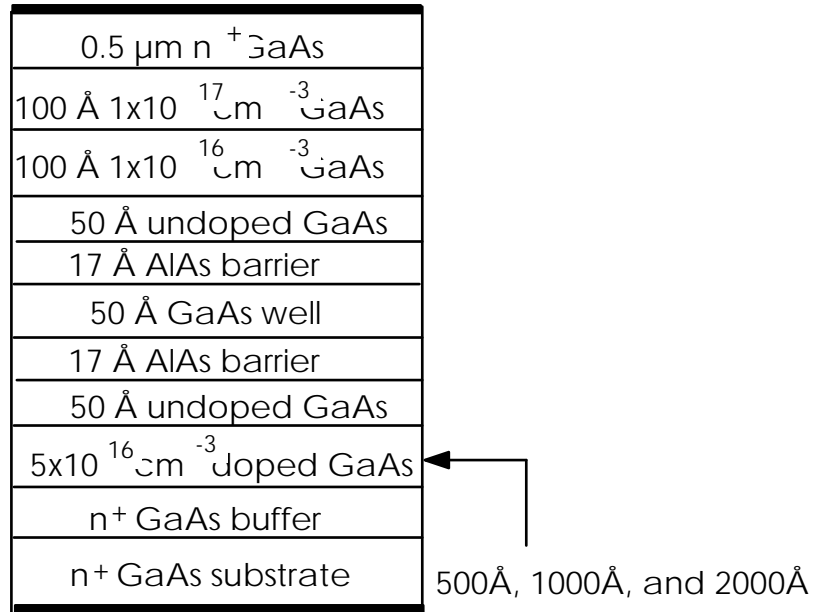


Fig. 4.1: A schematic cross section of the QWITT diode structures, A through D, examined in this study.

density through the device, and to also promote  $\Gamma(\text{GaAs})$ - $\Gamma(\text{AlAs})$  tunneling [72]. Due to the large  $\Gamma(\text{GaAs})$ - $\Gamma(\text{AlAs})$  conduction band discontinuity of 1.1 eV in this material system, increased  $\Gamma(\text{GaAs})$ - $\Gamma(\text{AlAs})$  tunneling as seen in thin AlAs barriers,

has been shown to produce improved peak-to-valley current ratios from GaAs-AlAs resonant tunneling diodes [73]. A 250Å thick GaAs spacer region consisting of a 100Å, n-type  $1 \times 10^{17} \text{ cm}^{-3}$  doped layer, followed by a 100Å, n-type  $1 \times 10^{16} \text{ cm}^{-3}$  doped layer, with a 50Å, unintentionally undoped p-type  $1 \times 10^{14} \text{ cm}^{-3}$  layer was used on the cathode side of the devices (Fig. 4.1). In addition, a baseline resonant tunneling diode structure, D, with the same quantum well layers and with the same 250Å GaAs spacer layer on either side of the device was grown. Devices were fabricated using the sequence of steps described in Chapter 3. Device diameters were typically 4-8  $\mu\text{m}$ , corresponding to a device area of  $1.25\text{-}5 \times 10^{-7} \text{ cm}^2$ . Continuous and pulsed (50% duty cycle) dc current-voltage characteristics at room temperature were measured.

Fig. 4.2 shows the room temperature dc I-V characteristics obtained from a resonant tunneling diode, sample D. The forward bias direction corresponds to electron injection from the top contact. The I-V characteristics in either bias direction are quite symmetric with a typical peak-to-valley current ratio of 3:1 and a peak current density of around 25  $\text{kA/cm}^2$ . The small asymmetry in both the peak voltage and peak current between the two bias directions is probably due to small changes in the doping level on either side of the quantum well. Due to the asymmetric structure of the QWITT diode (structures A through C), the dc I-V characteristics for the two bias directions are very different. In any negative resistance diode the voltage and current difference between peak and valley,  $\Delta V_{\text{pv}}$  and  $\Delta I_{\text{pv}}$ , must be as large as

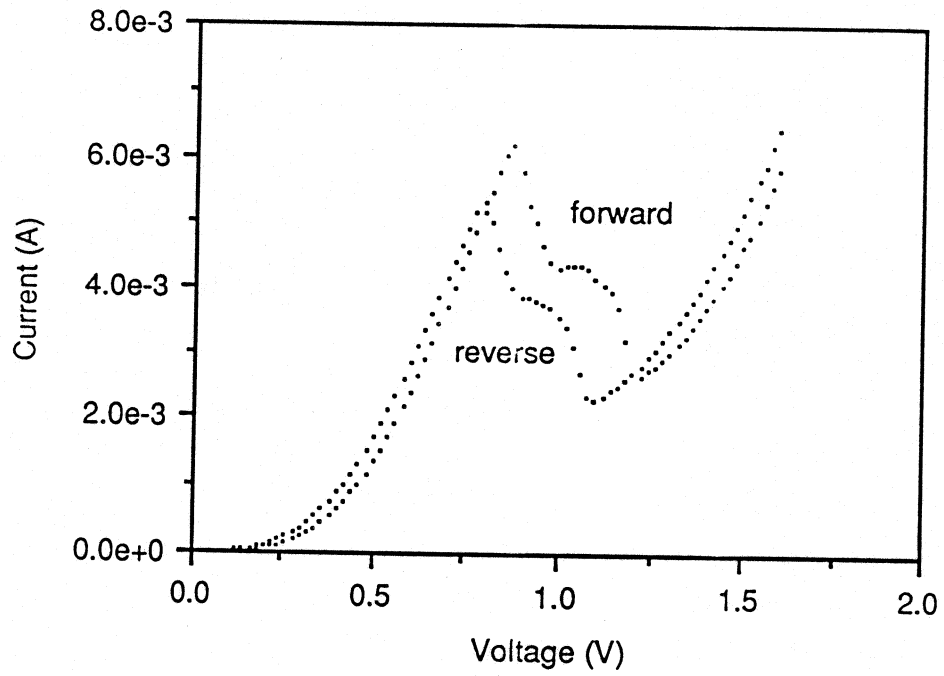


Fig. 4.2: Room temperature dc I-V curves in both bias directions for a resonant tunneling diode, device D.

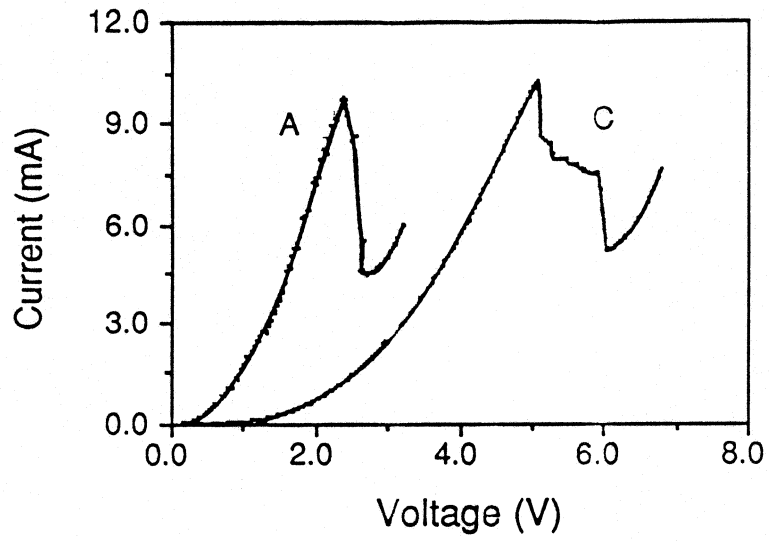


Fig. 4.3: Room temperature dc I-V curves for QWITT devices A and C with 500 Å and 2000 Å depletion region length respectively.

possible to increase the device output power; in a low frequency model power is directly proportional to  $\Delta V_{pv} \cdot \Delta I_{pv}$ . For the QWITT diode,  $\Delta V_{pv}$  is increased through the use of a drift region, but  $\Delta I_{pv}$  should remain virtually the same as the intrinsic quantum well. This results in an increase in the total output power that can be obtained from the QWITT diode compared to a bare resonant tunneling diode. The dc characteristics for the devices A through D are summarized in Table 4.1. For the QWITT bias mode (forward bias, substrate positive), as the length of the drift region is increased from 500Å to 2000Å, the voltage corresponding to the current peak,  $V_p$ , increases from 2.4V to 5.1V, and the voltage difference between peak and valley currents,  $\Delta V_{pv}$ , also increases from 0.3V to 1.1V (Fig. 4.3). We can see that while the variation in peak-to-valley current differences,  $\Delta J_{pv}$ , and peak current density,  $J_p$ , for the three devices A, B, and C, is quite small, large differences in  $\Delta V_{pv}$  are observed (Table 4.1&Fig. 4.3). Devices A and D have very similar voltage swings,  $\Delta V_{pv}$ , since the length of the depletion region in both these structures is almost the same. The increase in  $\Delta V_{pv}$  obtained through a proper choice of the depletion region length, also results in a corresponding increase in the specific negative resistance ( $\Delta V_{pv}/\Delta J_{pv}$ ) of the device. This suggests that the best oscillator performance in terms of output power would be obtained from device C. For this quantum well structure, when the depletion region length is increased much beyond 2000Å, the small signal and large signal analyses [64, 74] for the QWITT diode show that the voltage swing between peak and valley,  $\Delta V_{pv}$ , actually decreases due to the increased positive resistance in the device arising from both the space charge resistance and the undepleted portion of the drift region. This would then result in a degradation in the rf performance of the diode. For each device

Structure	$V_p$ (V)	$\Delta V$ (V)	$J_p$ kA/cm <sup>2</sup>	$\Delta J$ kA/cm <sup>2</sup>	peak to valley ratio	Specific Negative Resistance $\Omega$ -cm <sup>2</sup>
(A) 50Å spacer W = 500Å 5x10 <sup>16</sup>	2.5	0.3	26	12	1.8	2.6 x 10 <sup>-5</sup>
(B) 50Å spacer W = 1000Å 5x10 <sup>16</sup>	4.6	0.5	30	13	1.8	3.9 x 10 <sup>-5</sup>
(C) 50Å spacer W = 2000Å 5x10 <sup>16</sup>	5.1	1.0	28	14	2.0	6.8 x 10 <sup>-5</sup>
(D) symmetric RTD	0.88	0.34	20	11	2.3	3.1 x 10 <sup>-5</sup>

Table 4.1: DC characteristics for QWITT devices with uniformly doped depletion regions, A through D.

structure, when electrons are injected from the substrate to the top (reverse bias, substrate negative)  $\Delta V_{pv}$  is smaller as compared to when electrons are injected from the top to the substrate (forward bias). This is because in reverse bias the  $n^-$  GaAs drift region is under accumulation, and can add only positive series resistance to the device, thus reducing  $\Delta V_{pv}$ , as opposed to the QWITT mode, where this region actually contributes to the negative resistance of the device.

A systematic study of the variations in peak voltage and peak current due to the processing conditions and reproducibility of the device structure by MBE was undertaken. We found 10% variation in peak voltage from process induced changes, arising primarily from variations in the quality of the ohmic contacts, caused by small changes in the AuGe/Ni metallization scheme. InGaAs-based ohmic contacts [75] should significantly improve the ohmic contact reproducibility. Changes in nominally the same device structure from one MBE growth run to another was found to be within the 10% change in voltage due to processing variations. We have also found 20% variation in the peak current density arising primarily due to inaccuracy in the estimate of the device area.

## 4.2 Devices with Doping Spikes

For QWITT devices containing a uniformly doped depletion region, our self-consistent large signal model [74] indicates that the electric field in this region is of the order of 100 kV/cm. For GaAs, electric fields around 3-10 kV/cm are sufficient to have carrier velocities around  $10^7$  cm/sec. Hence, a doping spike at the beginning of the drift region could be introduced, much like in a lo-hi-lo IMPATT structure

[22], so that the electric field in the GaAs drift region is reduced and yet the entire drift region is fully depleted. This would then result in a reduction in the dc bias across the device and hence improve the dc-to-rf conversion efficiency. Since the entire drift region is still depleted the voltage swing between peak and valley would remain the same, and thus the rf output power will not be reduced compared to the uniformly doped drift region device. Fig. 4.4 shows a schematic of the device structures, E through H, examined in this study. Device E corresponds to the limiting case when the doping concentration in the spike equals the background doping of  $5 \times 10^{16} \text{ cm}^{-3}$  in the drift region. Devices F through H contain a  $100 \text{ \AA}$  GaAs doping spike of varying doping concentration from  $8 \times 10^{16} \text{ cm}^{-3}$  to  $5 \times 10^{17} \text{ cm}^{-3}$  at the beginning of the drift region followed by a  $1800 \text{ \AA}$  n- GaAs layer, doped  $5 \times 10^{16} \text{ cm}^{-3}$ . Note that the total thickness of the GaAs layers following the quantum well region on the anode side is constant at  $2000 \text{ \AA}$  from devices A through H (Figs. 4.1&4.4). All the device structures E through H have identical quantum well regions and cathode spacer layers. The dc characteristics of these devices, E through H, is summarized in Table 4.2. By changing the doping concentration in the spike from  $5 \times 10^{16} \text{ cm}^{-3}$  to  $5 \times 10^{17} \text{ cm}^{-3}$  the peak voltage is reduced from 3.5V in device E to 0.64V in device H. However, the voltage swing,  $\Delta V_{pv}$ , is also reduced from 1.1V to 0.34V, suggesting that the lightly doped GaAs drift region is not fully depleted. By reducing the spike doping concentration to  $1 \times 10^{17} \text{ cm}^{-3}$  in device G the voltage swing,  $\Delta V_{pv}$ , improves to 0.64V but this value is still lower than that seen in the uniformly doped device E. A further reduction in the spike doping concentration to

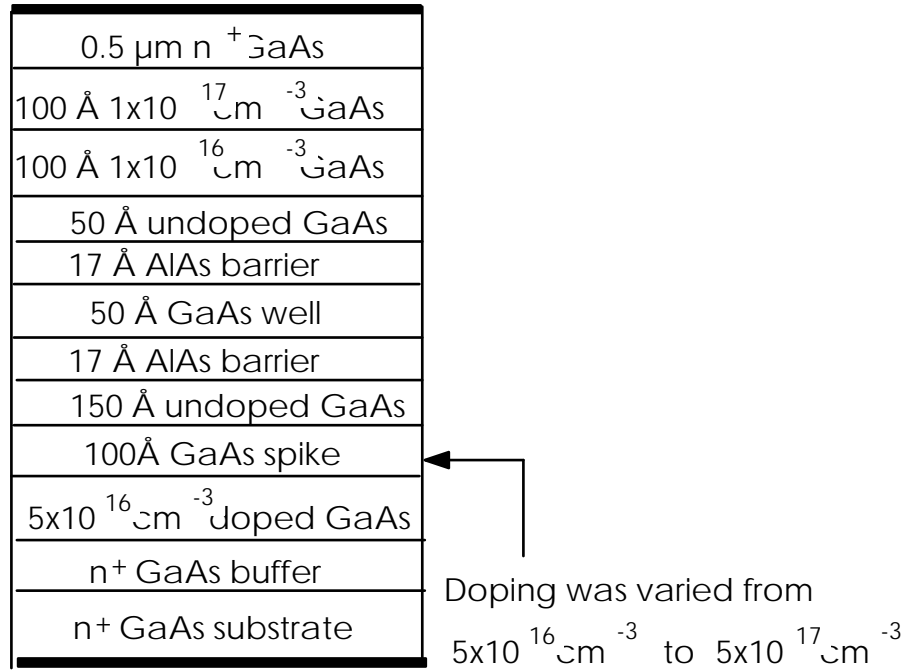


Fig. 4.4: A schematic cross section of the QWITT diode structures with a doping spike, E through H, examined in this study.

Structure	$V_p$ (V)	$\Delta V$ (V)	$J_p$ kA/cm <sup>2</sup>	$\Delta J$ kA/cm <sup>2</sup>	peak to valley ratio	Specific Negative Resistance $\Omega$ -cm <sup>2</sup>
(E) 100Å spike $5 \times 10^{16}$ W = 1800Å	3.5	1.1	31	19	2.5	5.8 x $10^{-5}$
(F) 100Å spike $8 \times 10^{16}$ W = 1800Å	2.6	1.2	28	17	2.6	7.0 x $10^{-5}$
(G) 100Å spike $1 \times 10^{17}$ W = 1800Å	0.9	0.64	23	12	2.1	5.3 x $10^{-5}$
(H) 100Å spike $5 \times 10^{17}$ W = 1800Å	0.64	0.34	21	12	2.3	2.8 x $10^{-5}$

Table 4.2: DC characteristics for QWITT devices with a doping spike, E through H.

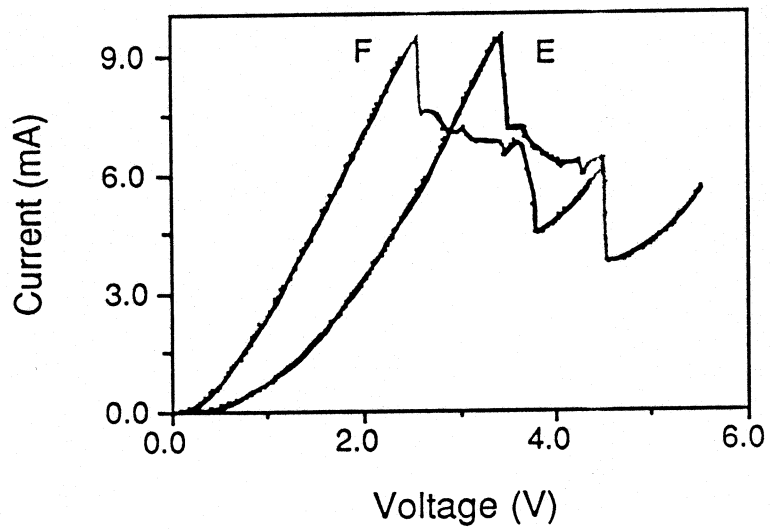


Fig. 4.5: Room temperature dc I-V curves for QWITT devices E and F with a doping spike of  $5 \times 10^{16} \text{ cm}^{-3}$  and  $1 \times 10^{17} \text{ cm}^{-3}$  respectively.

$8 \times 10^{16} \text{ cm}^{-3}$  in device F causes  $\Delta V_{pV}$  to recover to 1.2V. Note that the peak voltage in device F is about 30% lower compared to device E, but the voltage swing,  $\Delta V_{pV}$ , and the current swing,  $\Delta J_{pV}$ , for the two devices are similar. This suggests that the oscillator output power obtained from devices E and F should be the same, with device F having higher efficiency due to the lower dc bias obtained through the introduction of a doping spike. The dc I-V curves for devices E and F are shown in Fig. 4.5. As seen before in devices A through C, in the opposite bias direction when the drift region is under accumulation the increased series resistance in the device causes a reduction in the voltage swing,  $\Delta V_{pV}$ .

### 4.3 Conclusions

In summary, dc characteristics of different QWITT devices with both uniformly doped drift regions and with drift regions containing a doping spike have been presented. In order to obtain the best rf oscillator performance the importance of choosing a device structure that maximizes the  $\Delta V_{pV} \cdot \Delta I_{pV}$  product, is emphasized. As we shall see in the next chapter when characterizing QWITT diode oscillators at frequencies below the characteristic frequency,  $\sigma/2\pi\epsilon$  (this frequency is typically around 40 GHz for  $\sigma=0.3 \text{ mho/cm}$ ), the dc characteristics are a good measure of rf oscillator performance. This is consistent with the small signal analysis presented in Chapter 2 where we found that the specific negative resistance for a QWITT diode is essentially constant from dc up to frequencies around  $\sigma/2\pi\epsilon$ .